國 立 交 通 大 學

電信工程研究所

碩 士 論 文

三種具可調頻寬之雙模雙頻帶通濾波器

Three Dual-Mode Dual-Band Bandpass Filter Designs With Controllable Bandwidths

研究生：林祖偉

指導教授：郭仁財教授

中 華 民 國 九十九 年 七 月

三種具可調頻寬之雙模雙頻帶通濾波器

Three Dual-mode Dual-band Bandpass Filter Designs With Controllable Bandwidth

研究生：林祖偉 **Student:Tsu-Wei Lin**

指導教授：郭仁財 博士 **Advisor:Dr. Jen-Tsai Kuo**

國立交通大學

電信工程研究所

碩士論文

A Thesis
Submitted to Institute of Communication Engineering
College of Electrical and Computer Engineering
National Chiao Tung University
in Partial Fulfillment of the Requirements
for the Degree of
Master of Science
in
Communication Engineering
July 2010
Hsinchu, Taiwan, Republic of China

中華民國九十九年七月

三種具可調頻寬之雙模雙頻帶通濾波器

研 究 生：林 祖 偉　　指 導 教 授：郭 仁 財　博 士

國立交通大學電信工程研究所

摘要

本論文提出三種可調頻寬之雙模雙頻帶通濾波器。第一種利用步階阻抗諧振腔實現雙頻帶濾波器，並在諧振器中間接上一段短的接地高阻抗傳輸線，以提供電感性耦合。為增加設計自由度，一指叉式電容設計於諧振器的中央，即可控制兩通帶的頻寬與中心頻率。此外，進一步利用源端與負載端的耦合，以形成多個傳輸零點，增進兩通帶的頻率選擇度。此部份實作兩雙頻帶通濾波器，量測與模擬結果吻合。

本文第二種雙模雙頻帶通濾波器，利用雙端接地之步階阻抗諧振器，以兩段短的高阻抗線頭尾相接，以形成雙模雙頻帶通濾波器。藉由調整電感性耦合的大小，可控制兩頻段頻寬。除此之外，利用斜對稱饋入，以產生兩個傳輸零點，進而改善兩通帶的頻率選擇度。第三種雙模雙頻帶通濾波器使用與第二種帶通濾波器相同的諧振腔，但將其兩接地孔相互連結以形成單一的接地孔，可降低製作上的誤差，電路佈局可更為緊密並節省電路

面積。本電路亦可利用源端與負載端的耦合，產生多重傳輸零點，大幅提高兩通帶的頻率選擇度。此兩部分亦各實作兩個電路，以驗證設計理論，量測與模擬結果相當一致。

Three Dual-Mode Dual-Band Bandpass Filter Designs With Controllable Bandwidths

Student: Tsu-Wei Lin

Advisor: Dr. Jen-Tsai Kuo

Institute of Communication Engineering

National Chiao Tung University

Abstract

Three dual-mode dual-band bandpass filters are proposed in this thesis. The first dual-mode dual-band bandpass filter is devised based on a single stepped-impedance resonator. The center of the resonator is grounded through a short high-impedance section, which is equivalent to an inductor for providing coupling between the resonant modes. In addition, in order to increase the degree of freedom for dual-band design, an interdigital capacitor is introduced so that both center frequencies and bandwidths of two passband can be controlled. Moreover, with the aid of source-load coupling, two extra transmission zeros can be created close to the passband edges and hence greatly improve the frequency selectivity between the two passbands. Two filters are fabricated and measured to validate the proposed

idea. The measured results show good agreement with the simulation.

The second dual-mode dual-band bandpass filter is again designed based on two stepped-impedance resonators. Both ends of each resonator are terminated to the ground. For the dual-mode operation, the two stepped-impedance resonators are connected to the ground via by two short high-impedance sections. The inductive coupling is provided to control the bandwidths of the two passbands. With a skew symmetric feed structure, two transmission zeros are created between the two passbands. To obtain a simpler fabricated process and more compact circuit area, the third dual-mode dual-band bandpass filter is evolved from the second filter with two ground vias being connected to a single one. With the aid of source-load coupling, again, transmission zeros are generated to improved the selectivity of the two passbands. Two microstrip circuits are fabricated and measured to validate design ideas of the second and third bandpass filters. The simulation and measurement results show good agreement.

Acknowledgement

誌謝

本篇論文得以完成首要感謝指導教授郭仁財博士，在郭教授認真的指導下，使我得以體認研究的精神。感謝口試委員:吳瑞北教授、張志揚教授、林祐生教授，對學生的論文提供寶貴的意見。

感謝家人的支持，因為有你們的付出使我這一年半的求學生涯更加順遂。感謝陳逸名學長、邱逸群學長引領我進入微波電路設計領域，不厭其煩的為我解決研究上的問題。感謝裕豪學長的幽默，為實驗室帶來許多的歡笑，也感謝 908 實驗室一同奮鬥夥伴:宣融、詩薇、卓諭、峻瑜、紹展、麒宏，還有實驗室兩位學弟:孟修、祐先，你們的幫忙使我受惠良多。感謝大學時代的好友李銘晃和陳柏志，謝謝你們時常的關心。

Content

List of Figures

List of Tables

Chapter 1

Introduction

With the increasing demands for dual-band applications in modern wireless system such as the global systems for mobile communications (GSM) at 0.9/1.8 GHz and wireless local area networks (WLANs) at 2.4/5.2 GHz, research on innovative designs of dual-band filters has become very popular recently [1-16]. In [1-2], the dual-passband response is achieved by arranging the stepped-impedance resonator in parallel-coupled or inline configuration. In [3], four hairpin resonators in a 2×2 configuration are used to design quasi-elliptic function passbands at the two designated frequencies. In [4], a dual-band microstrip bandpass filter is developed using net-type resonators. By adding extra resonators, quasi-elliptic function response can be designed. In [5], a dual-band bandpass filter using parallel short-ended feed scheme is proposed. Source-load coupling is employed to create four transmission zeros to improve the frequency selectivity. In [6], pseudo-interdigital stepped-impedance resonators are employed to build the dual-band filter. In [7-8], a resonator loaded with a stub is adopted to implement the dual-band characteristics. In [9], a systematic synthesis procedure is presented for a dual-band filter with fully controllable second passband. On the basis of the idea in [9], flexible passband and bandwidth selections can be achieved by utilizing a stepped-impedance coupled-line as a dual-band inverter [10].

Dual-mode resonators are suitable for designing dual-band filters with a compact size. In [11], two microstrip dual-mode rings on different layers form a stacked-loop structure and each ring controls one passband. This idea is also extended to the coplanar waveguide (CPW) structure [12]. In [13], the feed lines are placed between two loop resonators to offer sufficient coupling for both passbands. The dual-band filter in [14] is designed in a multilayer structure consisting of dual-mode resonators in a reflector cavity. It is noted that each selected passband in [11]-[14] is mainly controlled by a resonator, so that two resonating elements are required.

In [15], a dual-band bandpass filter is implemented based on non-degenerate dual-mode slow-wave open-loop resonator. Moreover, different feed schemes are discussed in this paper. In [16], a dual-mode dual-band bandpass filter uses a single ring resonator consisting of several microwave *C*-sections; each of them is used to substitute a λ/4- or λ/6-section of a traditional ring.

In this thesis, three dual-mode dual-band bandpass filters are presented. The first one was presented in [17]. In Chapter 2, a new dual-band filter is devised by a single stepped-impedance resonator. The center of the resonator is connected to a ground via through a short high-impedance section, providing inductive coupling to the resonating modes [18-20]. Besides, an interdigital structure is inserted in shunt with the inductive sections to establish proper capacitive coupling for the resonant modes. With these two types of coupling, center frequencies and bandwidths of the two passbands can be controlled. Furthermore, with the aid

of source-load coupling, two extra transmission zeros are created to improve the filter selectivity in the band rejection between the two passbands.

In Chapter 3, an alternative dual-mode dual-band bandpass filter is investigated. The resonant element is stepped-impedance resonator with both ends being terminated to the ground by two short high-impedance sections. In this way, sufficient inductive coupling can be established between the resonant modes. Besides, skew symmetric feed structure is applied in this filter so that two transmission zeros can be created between the two passbands.

There are two grounding vias in the dual-mode dual-band bandpass filter in Chapter 3. These two vias may cause large fabrication errors. Thus, in Chapter 4, the two separated ground vias are connected to a single one to ease the fabrication and reduce the circuit area. Again, the source-load coupling is employed to generate several transmission zeros to enhance the filter selectivity near the two passbands.

Finally, conclusion of this thesis is drawn in Chapter 5.

Chapter 2

Dual-mode dual-band bandpass filter (I)

Fig. 2-1(a) shows the layout of the first dual-mode dual-band filter. In this demonstration, the two center frequencies are f_1 = 2.45 GHz and f_2 = 5.2 GHz. The circuit is evolved from a stepped-impedance resonator configured as a cascade of two high-impedance sections with a low-impedance section in between. Let the characteristic impedances of the high- and low-impedance sections be Z_1 and Z_2, and electrical lengths at f_1 be θ_1 and θ_2, respectively. The equivalent circuit for modeling the interdigital capacitor consists of three capacitors in a π-circuit, and that for the high-impedance sections and the ground via is a T-network with three inductors, as shown in Fig. 2-1(b). Since the value of C_2 is small, it is neglected in the following analysis.

2.1 Resonant frequency

The resonant frequencies of the stepped-impedance resonator are primarily determined by the length ratio $\theta_2/(\theta_1 + \theta_2)$ and impedance ratio Z_1/Z_2 and can be calculated by the transmission line theory [1-2]. In order to obtain the dual-band characteristic, the first higher order resonance of the resonator is utilized to form the second passband. Fig. 2-3 depicts the resonant spectrum with respect to the fundamental frequency. In our case, the frequency ratio

of f_2 over f_1 is 2.122. To meet the required frequency ratio, the electrical ratio can be selected to 0.592 and impedance ratio can be selected to 3. Due to the symmetry of Fig. 2-1(a), we may use the even-mode and odd-mode analyses to calculate the resonant frequencies. The even and odd mode equivalent circuits of Fig. 2-1(a) are depicted in Fig. 2-2(a) and Fig. 2-2(b), respectively. When Y_{ine} and Y_{ino} are equal to zero, the resonant frequencies of the circuit in Fig. 2-1(a) can be calculated by the following equations:

Even-mode:

$$\omega(L_1 + 2L_2)(Z_1 \tan\theta_2 + Z_2 \tan\theta_1) + Z_1^2 \tan\theta_1 \tan\theta_2 - Z_1 Z_2 = 0 \qquad (2.1)$$

Odd-mode:

$$Z_1^2 \tan\theta_1 \tan\theta_2 - Z_1 Z_2 + \frac{\omega L_2 \left(Z_1 \tan\theta_2 + Z_2 \tan\theta_1\right)}{1 - 2\omega^2 C_1 L_2} = 0 \qquad (2.2)$$

2.2 Extraction of equivalent inductor and capacitor values

The equivalent inductance for an electrically short high-impedance section of the Fig.2-1(a) can be easily derived. However, the parasitics of the ground via should be included here, so that extraction for the values of L_1 and L_2 in the T-model is required. The Z-matrix of the T-model can be derived as

$$[Z]=\begin{bmatrix} Z_{11} & Z_{12} \\ Z_{21} & Z_{22} \end{bmatrix}= j\omega\begin{bmatrix} L_1+L_2 & L_2 \\ L_2 & L_1+L_2 \end{bmatrix} \tag{2.3}$$

where ω is the operating angular frequency, Z_{11} = Z_{22} and Z_{12} = Z_{21}. Similarly, the *S*-parameters of the distributed inductor can be obtained from the EM simulator [23], and can be written as

$$[S]=\begin{bmatrix} S_{11} & S_{12} \\ S_{21} & S_{22} \end{bmatrix} \tag{2.4}$$

The transformations from *S*-parameters to the *Z*-parameters [25] can be written as

$$Z_{11}=Z_0\frac{(1+S_{11})(1-S_{22})+S_{12}S_{21}}{(1-S_{11})(1-S_{22})-S_{21}S_{12}} \tag{2.5}$$

$$Z_{12}=Z_0\frac{2S_{12}}{(1-S_{11})(1-S_{22})-S_{21}S_{12}} \tag{2.6}$$

Then, using (2-3) to (2-6), the values of L_1 and L_2 can be extracted. For a substrate with ε_r = 2.2 and thickness = 0.508 mm, L_1 and L_2 are about 0.5 and 0.2 nH, when L_t = W_t = 0.3 mm, W_{c2} = 0.2 mm, L_{c1} + L_{c2} = 1.7 mm and *r* (radius of the ground via) = 0.2 mm. Fig. 2-4 shows the inductor values versus the operating frequencies from 1 GHz to 7 GHz. It can be observed that the variations of L_1 and L_2 with respect to operating frequencies are quite small. The equivalent circuit for the interdigital structure is a π network with the three capacitors. If C_2

neglected, only C_1 value needs to be calculated. The approximated value of the capacitor C_1 can be obtained from the following empirical equations [24], when L_{c1} = 1.5 mm, W_{c1} = 0.15 mm, N = 5, h = 0.508mm, and ε_r = 2.2.

$$C_1 \approx (\varepsilon_r + 1)\ell_{c1}[(N-3)A_1 + A_2] \approx 0.0765\,pF \tag{2.7}$$

where

$$A_1 = 4.409\tanh\left[0.55\left(\frac{h}{W_{c1}}\right)^{0.45}\right]\times 10^{-6}\,(pF/\mu m)$$
$$A_2 = 9.92\tanh\left[0.525\left(\frac{h}{W_{c1}}\right)^{0.5}\right]\times 10^{-6}\,(pF/\mu m) \tag{2.8}$$

This is an important step in our design since the bandwidths of the dual-passband response are controlled by these element values. Given the values of L_1, L_2 and C_1, the resonant frequencies of the circuit can be obtained by solving (2.1) and (2.2).

2.3 Control of bandwidths

The solutions to (2.1) and (2.2) are initial data for designing the circuit in Fig. 2-1(a). Fig. 2-5 shows the typical frequency responses for extracting the resonant frequencies from simulation. All geometric parameters are in Fig. 2-9, except that a gap with a size of 0.1 mm

is inserted between the circuit and the input and output ports. Four resonances can be observed. The bandwidth and coupling coefficient relations of the dual-mode dual-band bandpass filter are as shown as following equations:

The first passband:

$$k_1 = \frac{2|f_a - f_b|}{f_a + f_b} = \frac{BW_1}{f_{c1}\sqrt{g_1 g_2}} \tag{2.9}$$

The second passband:

$$k_2 = \frac{2|f_c - f_d|}{f_c + f_d} = \frac{BW_2}{f_{c2}\sqrt{g_1 g_2}} \tag{2.10}$$

where the f_{c1} and f_{c2} are the two center frequencies, g_1 and g_2 are element values of the lowpass prototype. The above equations indicate that both bandwidths can be controlled by varying four resonant modes. Fig. 2-6(a) and Fig. 2-6(b) show the changes of the four resonant frequencies versus the changes of L_t and L_{c1}, respectively. Here, the resonator has an impedance ratio Z_2/Z_1 = 5, a length ratio $\theta_2/(\theta_1+\theta_2)$ = 0.645, and eleven interdigital fingers. The corresponding parameters evaluated at f_1 = 2.45 GHz are Z_1 = 136.25 Ω, Z_2 = 27.25 Ω, θ_1 = 43.6°, and θ_2 = 79.21°. In Fig. 2-6(a), when the short high-impedance section L_t is varied from 0.2 to 0.7 mm, the resonant peaks at f_a and f_c shift to the lower frequencies, whereas the peaks at f_b and f_d remain almost unchanged. In Fig. 2-6(b), when L_{c1} is varied from 1.0 to 1.5

mm, the peak at f_d shifts to lower frequencies, whereas the other three resonances remain almost unchanged. Combining these two effects, the two bandwidths at the two designated frequencies can therefore be adjusted by choosing suitable L_t and L_{c1} values. It is noted that the center frequency of the first passband is defined as the arithmetic mean of f_a and f_b, and that of the second is the mean of f_c and f_d.

2.4 Control of transmission zeros

Each $|S_{21}|$ response in Fig. 2-7(a) possesses four transmission zeros. The variation of these zeros versus the length of source-load coupled section is studied in Fig. 2-7(b) Such coupled-line section between the input and output ports is capable of providing one more signal path from the source to the load, and it can be used to generate extra transmission zeros [22]. The even and odd mode characteristic impedances of this coupled-line are Z_{oe} = 181.3 Ω and Z_{oo} = 92 Ω, respectively. It can be seen from Fig. 2-7(b) that only when L_C is greater than 0.8 mm, two extra transmission zeros at f_{Z2} and f_{Z3} can be generated. It is noted that when L_C is increased, the four transmission zeros get closer to the passbands.

2.5 Simulation and measurement

Two dual-mode dual-band bandpass filters designed at f_1 = 2.45 GHz and f_2 = 5.2 GHz are fabricated and measured to validate the proposed design. The circuits are realized on a substrate with ε_r = 2.2 and h = 0.508 mm. Fig. 2-8(a) shows the simulated and measured responses of the first filter. Note that both passbands possess quasi-elliptic function responses. The measured insertion losses at f_1 and f_2 are 2.1 dB and 1.2 dB, respectively, and the inband return losses are better than 15 dB. The two fractional bandwidths are 6.5% and 14%. The stopband rejection level between the two passbands is better than -30 dB. The circuit photo is shown in Fig. 2-8(b). Note that in Fig. 2-8(a), the second fractional bandwidth is more than twice that of the first one. Making the bandwidth of second passband smaller, based on the results in Fig. 2-6, one can decrease the inductive coupling or increase the capacitive coupling shown in Fig. 2-1(b). To increase the capacitance C_1, the width of the grounded section W_{c1} of the resonator is increased so that more interdigital fingers can be realized. Note that the length ratio of the resonator has to be changed accordingly to keep f_1 and f_2 unchanged. Fig. 2-9(a) shows the simulated and measured results of the second filter. The fractional bandwidths of the first and the second passbands are 5.9% and 6.2%, respectively. The measured $|S_{21}|$ at f_1 and f_2 are -2.5 dB and -2.0 dB, respectively, and $|S_{11}|$ are better than -15 dB. Fig. 2-9(b) shows the circuit photo. The measured results show good agreement with the simulation response.

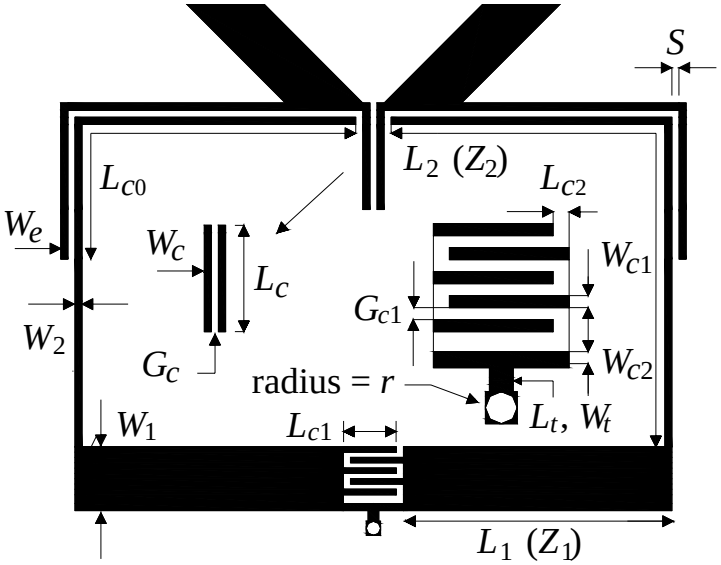

(a)

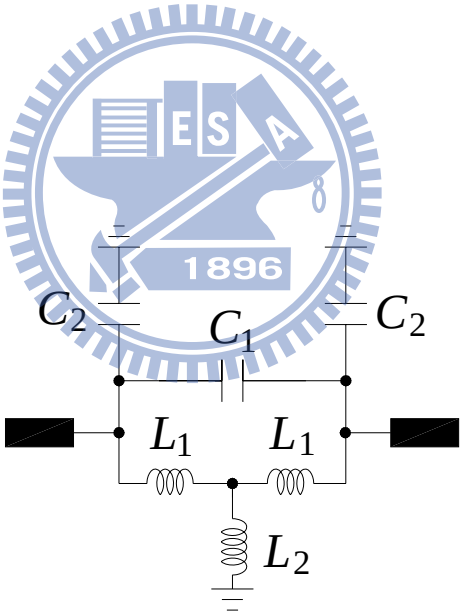

(b)

Fig. 2-1 (a) Circuit layout of the first proposed dual-mode dual-band filter. (b) Equivalent circuit of the interdigital capacitor and the ground via connected with short high-impedance sections.

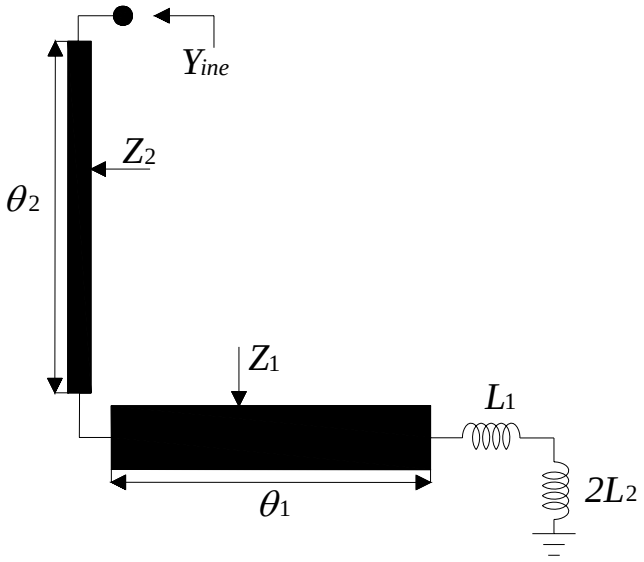

(a)

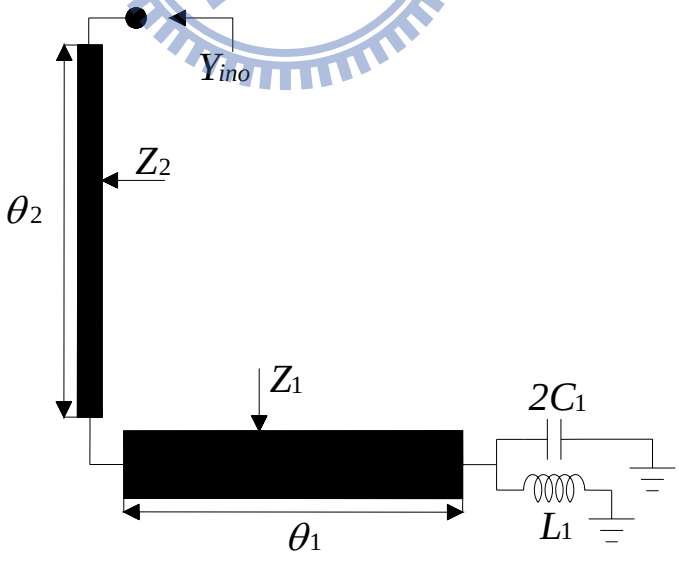

(b)

Fig. 2-2 (a) Even-mode equivalent circuit of Fig. 2-1(a). (b) Odd-mode equivalent circuit of Fig. 2-1(a)

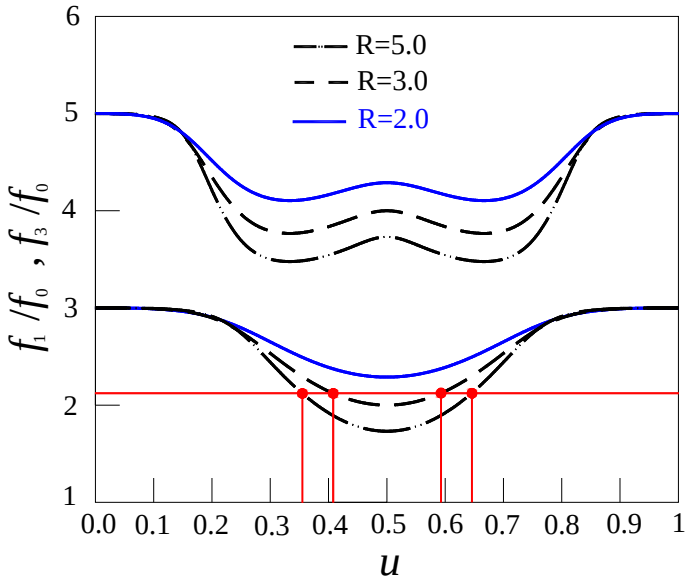

Fig. 2-3 Normalized resonant spectrum. f_0 is the fundamental frequency of a uniform (R = 1) resonator.

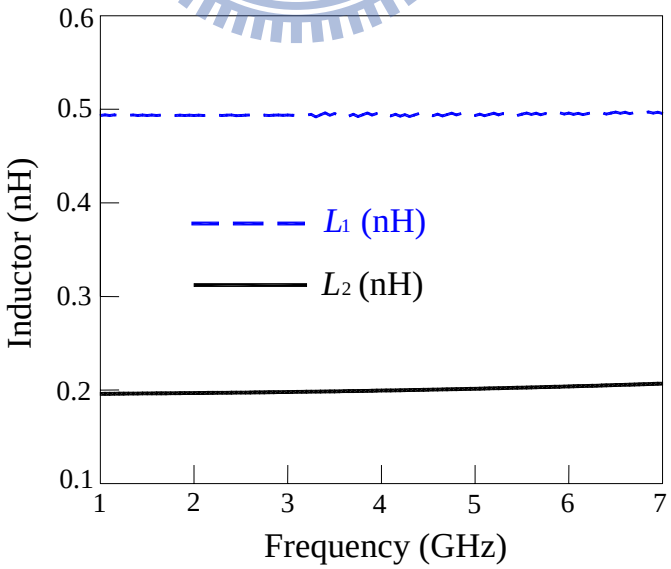

Fig. 2-4 Values of L_1 and L_2.

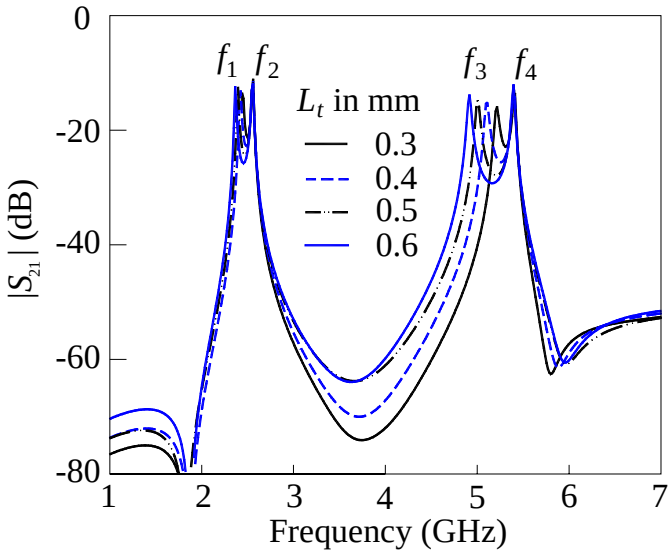

Fig. 2-5 Changes of resonant frequencies with variation of L_t. Detailed parameters are in Fig. 2-9.

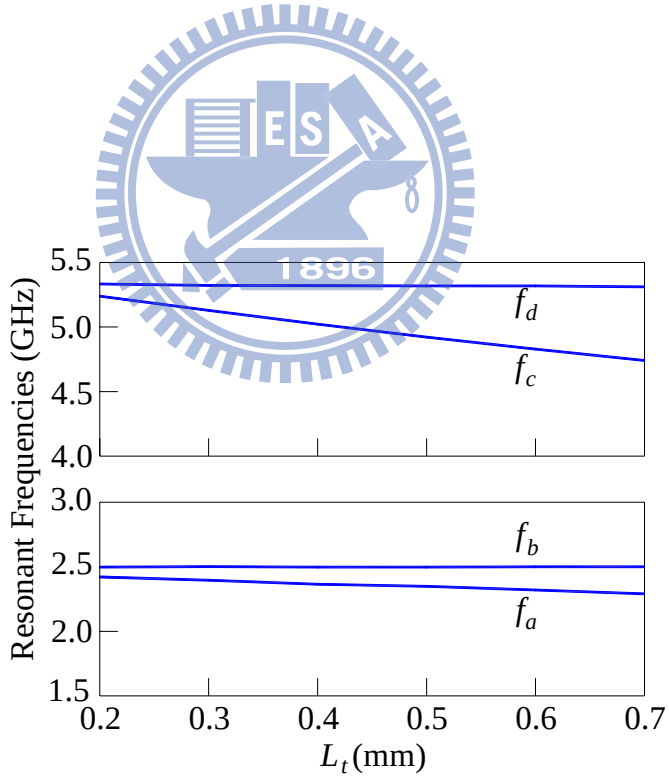

(a)

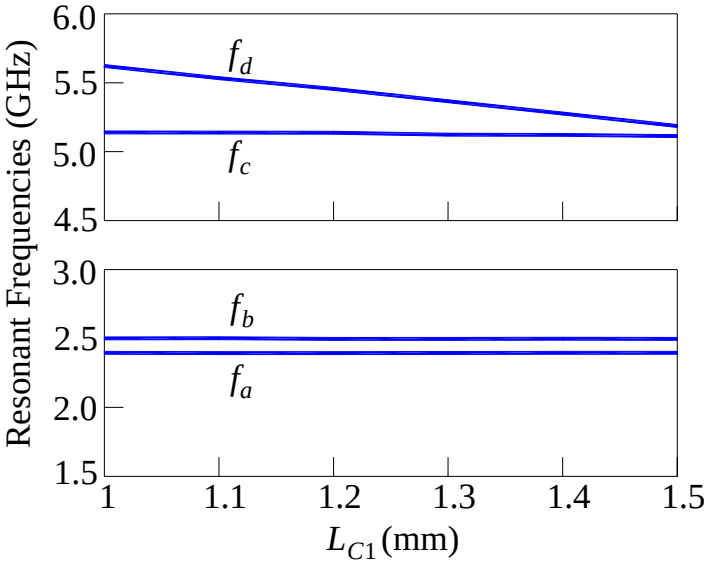

(b)

Fig. 2-6 (a) Resonant frequencies versus L_t with L_{c1} = 1.5 mm. (b) Resonant frequencies versus L_{c1} with L_t = 0.3 mm. Geometric parameters in mm: W_t = 0.3, W_{c2} = 0.2, W_{c1} = G_{c1} = 0.15, L_{c1} = 1.5, r = 0.2.

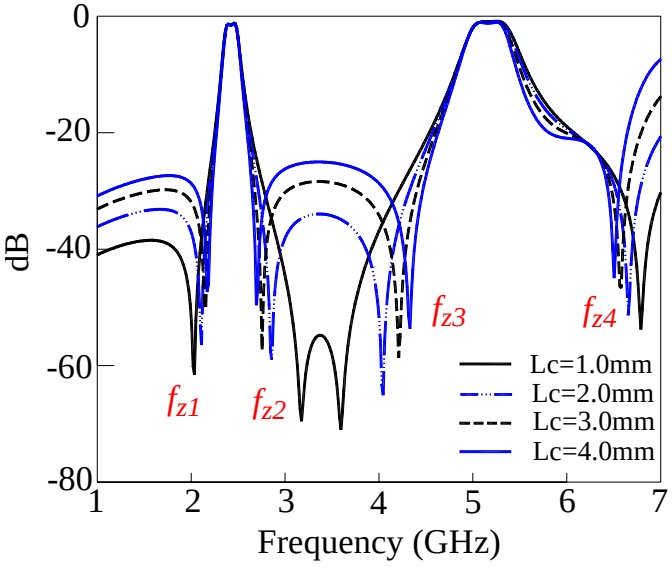

(a)

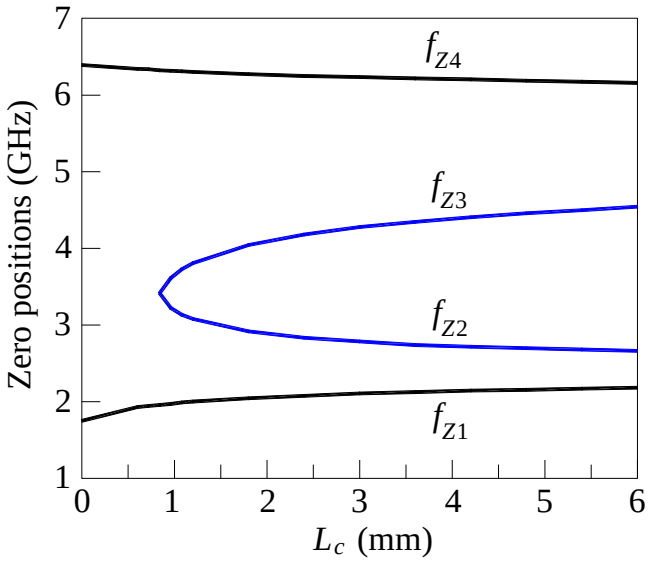

(b)

Fig. 2-7 (a) Change of the four transmission zeros versus the length of source-load coupled section, L_c. (b) The design curve of the four transmission zeros versus the length of source-load coupled section, L_c.

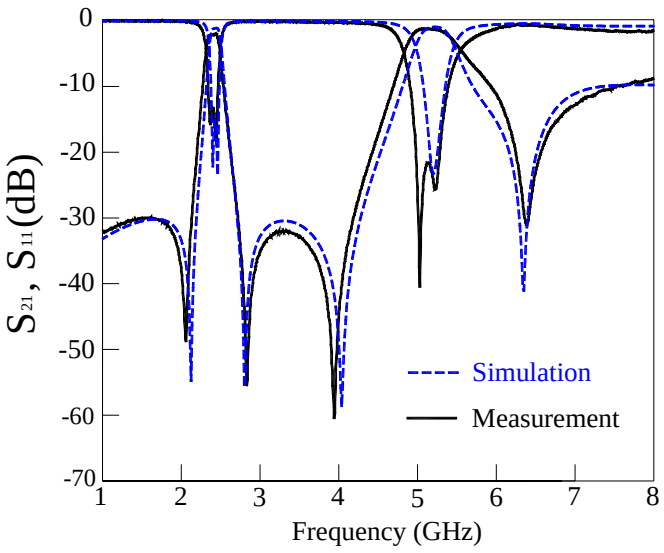

(a)

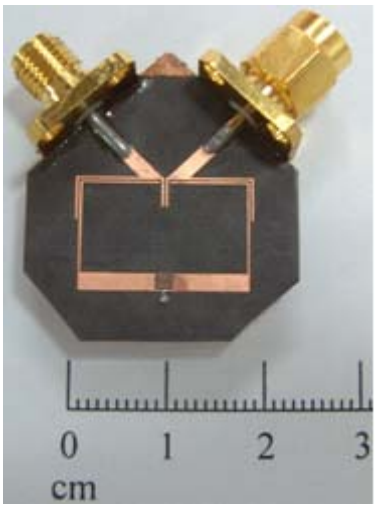

(b)

Fig. 2-8 (a) Simulation and measured results. (b) Circuit photo. Geometric parameters in mm: L_1 = 7.6, W_1 = 1.8, L_2 = 16.85, L_{c0} = 12.65, W_t = L_t = 0.3, W_2 = W_{c2} = W_e = S = G_c = L_{c2} = r = 0.2, W_{c1} = G_{c1} = 0.15, L_c = 3.0, L_{c1} = 1.5. Number of interdigital fingers = 5.

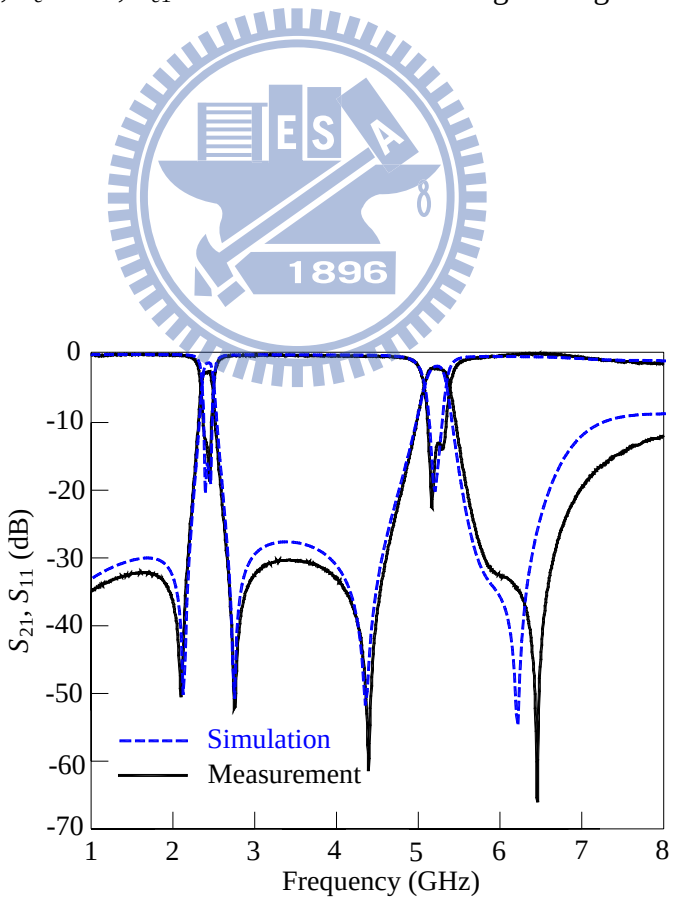

(a)

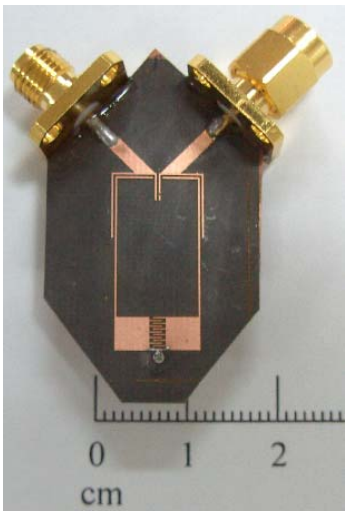

(b)

Fig. 2-9 (a) Simulation and measured responses of the second filter. (b) Circuit photo. Geometric parameters in mm: L_1 = 3.7, W_1 = 3.56, L_2 = 18.55, L_{c0} = 12.15, W_t = 0.3, L_t = 0.3, W_{c2} = G_c = r = W_2 = 0.2, W_{c1} = G_{c1} = 0.15, L_c = 3.0, L_{c1} = 1.35, L_{c2} = 0.35. Number of interdigital fingers = 11.

Chapter 3

Dual-Mode dual-band bandpass filter (II)

Fig. 3-1 shows the second dual-mode dual-band bandpass filter with two transmission zeros by applying the skew feed-in structure. In this demonstration, two center frequencies are f_1 = 2.45 GHz and f_2 = 5.8 GHz. The resonant element is stepped-impedance resonator of its both ends which are terminated to the ground. The circuit structure has two characteristic impedances Z_1 and Z_2, and electrical lengths at f_1 are $\theta_1 = \theta_{1a} + \theta_{1b}$ and θ_2, respectively. In Fig. 3-2, the equivalent circuit for modeling a short high impedance section and the ground via is a shunt inductor so that the inductive coupling is provided between the resonant modes. It is noted that capacitor C_0 represent the input and output coupling.

3.1 Resonant frequency

The resonant frequencies of the stepped-impedance resonator are primarily determined by the electrical length ratio $u = \theta_2/(\theta_1 + \theta_2)$ and impedance ratio $R = Z_1/Z_2$ and can be calculated by the transmission line theory. Since the two ends of this resonator are terminated to ground, the resonant conditions of this stepped-impedance resonator are the duality case in [1-2]. By using simple root searching program, the resonant spectrum can be calculated as shown in Fig.

3-3 where the higher-order resonant frequencies are normalized with respect to the fundamental frequency f_1. It is worth mentioning that Fig. 3-3 shows important design curve for dual-band operation. Since this structure is symmetric, the even and odd mode analyses can be used to calculate the resonant frequencies. The even-mode and odd-mode equivalent circuits of Fig. 3-1 are shown in Fig. 3-4(a) and Fig. 3-4(b), respectively. In Fig. 3-4(a), the input admittance for the even mode half circuit can be written as

$$Y_{ine} = Y_{ine1} + Y_{ine2} \tag{3.1}$$

When Y_{ine} is equal to zero, the even-mode resonant frequency can be derived as

$$Z_2\left(Z_1 - Z_2 \tan\theta_1 \tan\theta_2\right) - \omega L\left(Z_1 \tan\theta_2 + Z_2 \tan\theta_1\right) = 0 \tag{3.2}$$

In Fig. 3-4(b), let $L_1 = L_2$, and the input admittance for the even mode half circuit can be written as

$$Y_{ino} = Y_{ino1} + Y_{ino2} \tag{3.3}$$

When Y_{ino} is equal to zero, the odd-mode resonant frequency can be obtained by solving

$$Z_2 \tan\theta_1 \tan\theta_2 - Z_1 = 0 \tag{3.4}$$

3.2 Extraction of the equivalent inductor values

The equivalent circuit for the distributed inductor is a shunt inductor between the two resonators as shown as Fig. 3-2, and it is the important factor for determining the center frequency and bandwidth. The equivalent inductance for an electrically short high-impedance section and ground via can be derived as shown in section 2.2. For a substrate with ε_r = 2.2 and thickness = 0.508 mm, $L_1 = L_2$ is about 0.276 nH, when $L_{t1} = L_{t2}$ = 0.4 mm, $W_{t1} = W_{t2}$ = 0.2 mm, and r (radius of the ground via) = 0.2 mm. After the values of L_1 and L_2 are known, the resonant frequencies can be obtained by solving (3.2) and (3.4).

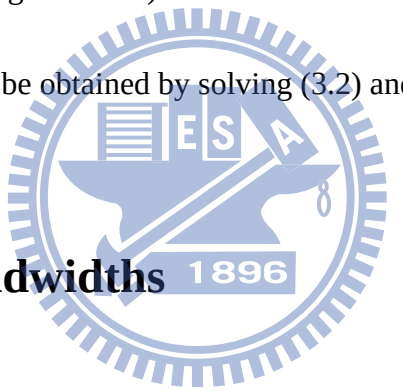

3.3 Control of bandwidths

Fig. 3-5 shows the frequency responses for validating the resonant frequencies of equations (3.2) and (3.4) from EM simulation [19]. All geometric parameters are in Fig. 3-10, except that a gap with a size of 0.1 mm is inserted between the circuit and the input and output ports. It has a total of four resonant peaks f_1, f_2, f_3, and f_4. According to (2-9) and (2-10), the bandwidths control can be achieved by adjusting the four resonant modes. Here, the resonator has impedance ratio Z_2/Z_1 = 2.0 and length ratio $\theta_2/(\theta_1+\theta_2)$ = 0.395. The corresponding parameters evaluated at f_1 = 2.45 GHz are Z_1 = 65 Ω, Z_2 = 130 Ω, θ_1 = 43°, and

$\theta_2 = 28^o$. In Fig. 3-6, when the short high-impedance section $L_t = L_{t1} = L_{t2}$ is varied from 0.2 to 1.0 mm, the resonant peaks at $f_1$and f_3 shift to the lower frequencies, whereas the peaks at f_2 and f_4 remain almost unchanged. Using the above mechanism, the two bandwidths at the two designated frequencies can be adjusted by choosing suitable L_{t1} and L_{t2} values. It is noted that the center frequency of the first passband is defined as the arithmetic mean of f_1 and f_2, and that of the second is the arithmetic mean of f_3 and f_4.

3.4 Control of transmission zeros

To increase the selectivity of the two passbands, a skew symmetric feed structure is applied to this structure. In [21], the zero degree feed structure is applied to generate additional transmission zeros. The similar idea will be applied to create transmission zeros here. Fig. 3-7 shows two different feed structures which are skew and symmetric feed structure, respectively. In Fig. 3-8, using the skew symmetric feed structure has two transmission zeros which are between the second passbands; however, in the symmetric feed structure, there are no transmission zeros between the two passbands. The equivalent circuit of the skew symmetric feed structure, in Fig. 3-2, indicates that there are two different signal paths from the input to the output port. Therefore, it has two transmission zeros around 4.67 GHz and 6.47 GHz, when $L_1 = L_2 = 0.276$ nH, $Z_1 = 65\ \Omega$, $Z_2 = 130\ \Omega$, $\theta_1 = 52^o$, $\theta_{1a} = 31^o$ and

$\theta_2 = 30^o$. For the skew symmetric feed structure, Fig. 3-9 depicts the variation of these zeros with the respect to the different feed locations. Three different feed locations are listed in the table 3.1. It is noted that the relation of $L_{e3} + L_{e4} = 16.96$ mm is satisfied in Feed A, Feed B and Feed C.

Feed	A	B	C
L_{e3} (mm)	11.73	10.73	9.73
L_{e4} (mm)	5.23	6.23	7.23

Table 3.1 Feed locations of different types

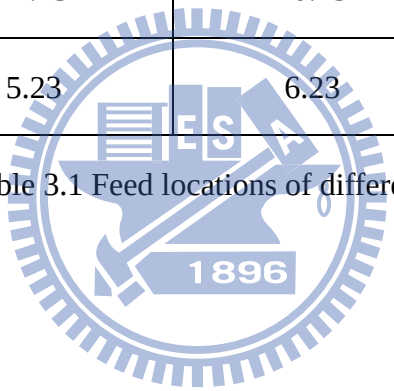

3.5 Simulation and measurement

A dual-mode dual-band bandpass filter is fabricated to validate the proposed idea. The center frequencies of the experimental circuit are $f_1 = 2.45$ GHz and $f_2 = 5.8$ GHz. A substrate with $\varepsilon_r = 2.2$ and $h = 0.508$ mm is used to build the circuits. Fig. 3-10 (a) shows the simulated and measured responses. The measured data show that the insertion losses at f_1 and f_2 are 2.15 dB and 2.91 dB, respectively, and the inband return losses are better than 15 dB. The two

fractional bandwidths are 5.8% and 3.8%, respectively. The circuit photo is in Fig. 3-10 (b), and the circuit size is 15.44 × 21.8 mm^2 ($0.17\lambda_g \times 0.24\lambda_g$). Simulation and measurement show good agreement.

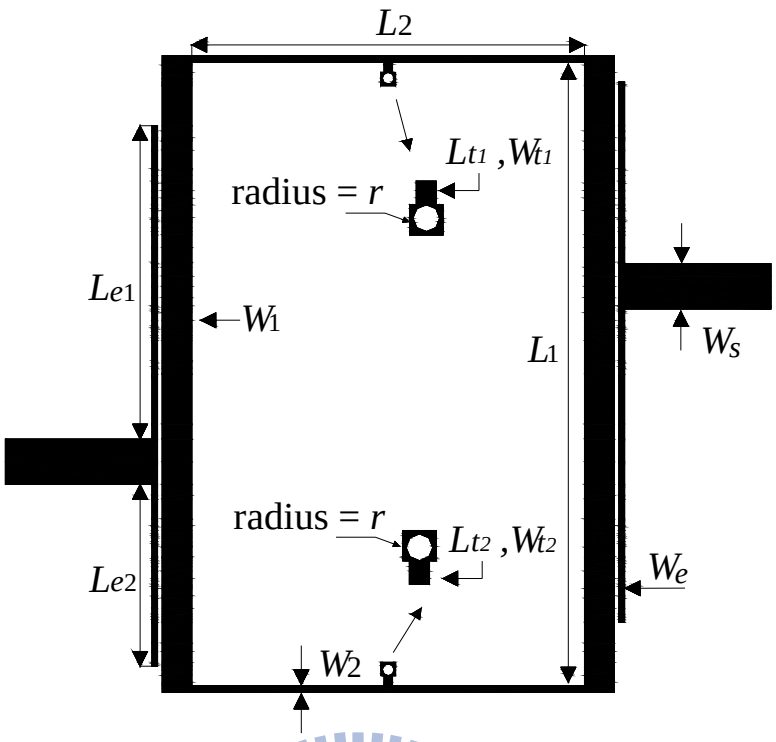

Fig. 3-1 Circuit layout of the second proposed dual-mode dual-band filter.

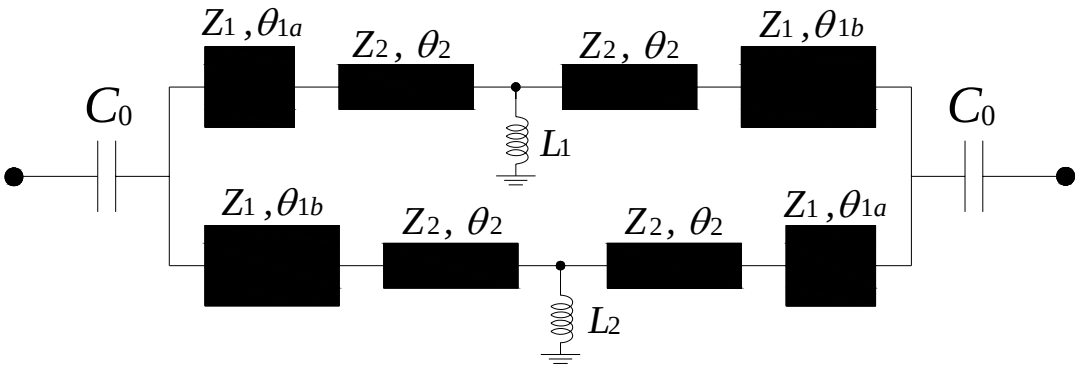

Fig. 3-2 Equivalent circuit of the entire circuit.

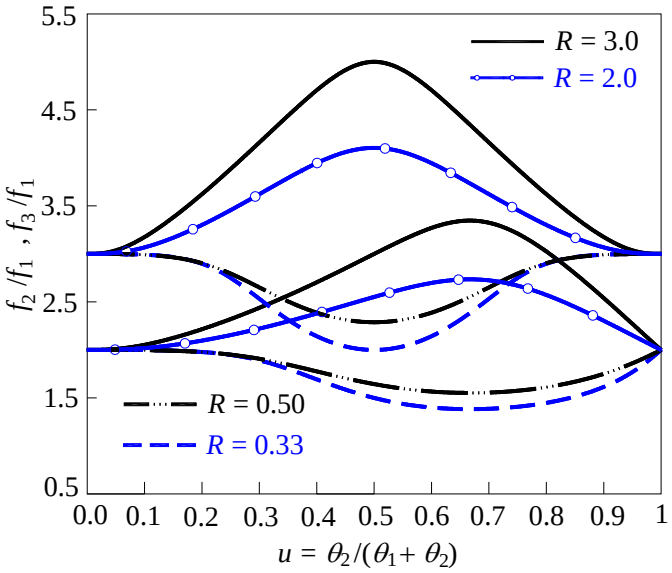

Fig. 3-3 Resonant spectrum normalized with respect to the fundamental frequency

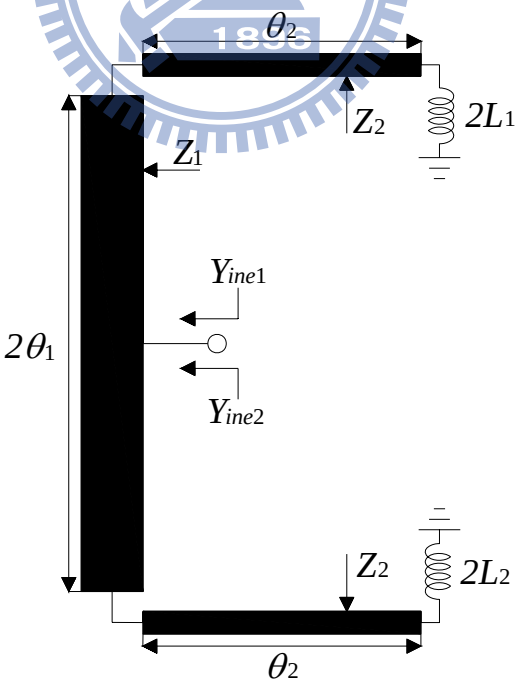

(a)

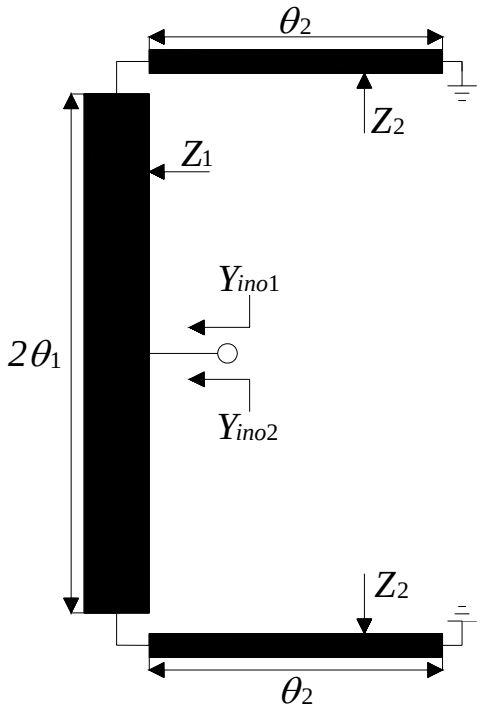

(b)

Fig. 3-4 (a) Even-mode equivalent circuit of Fig. 3-1(a). (b) Odd-mode equivalent circuit of Fig. 3-1(a)

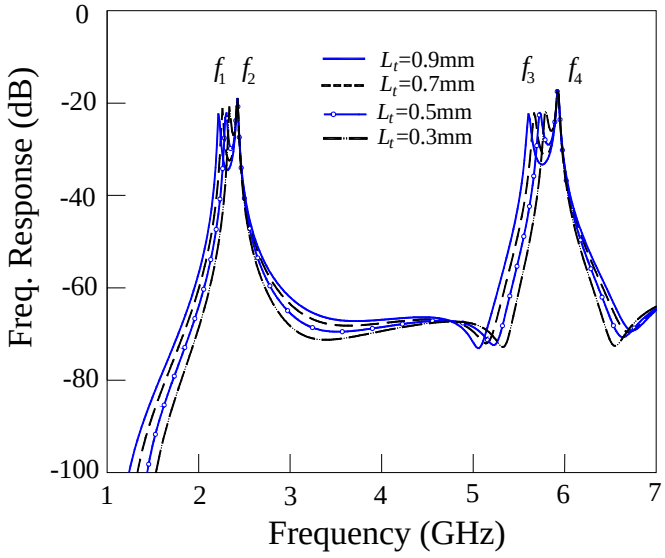

Fig. 3-5 Changes of resonant frequencies with variation of L_t. Detailed parameters are in Fig. 3-10.

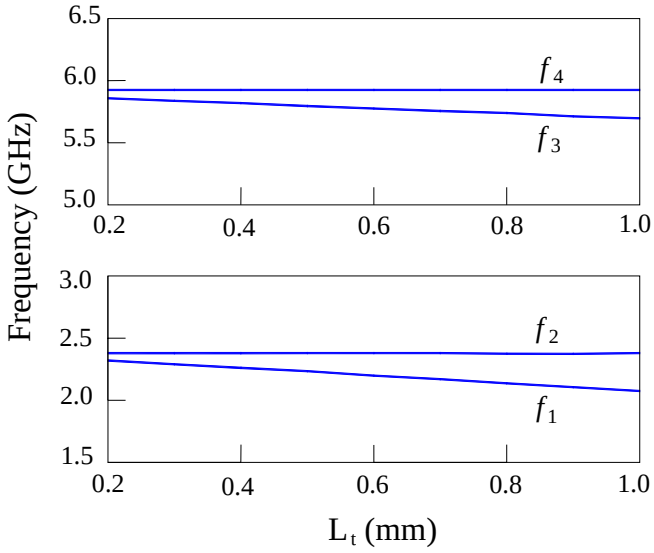

Fig. 3-6 Resonant frequencies versus $L_{t1} = L_{t2} = L_t$. Geometric parameters in mm: $W_t = 0.3$, $r = 0.2$.

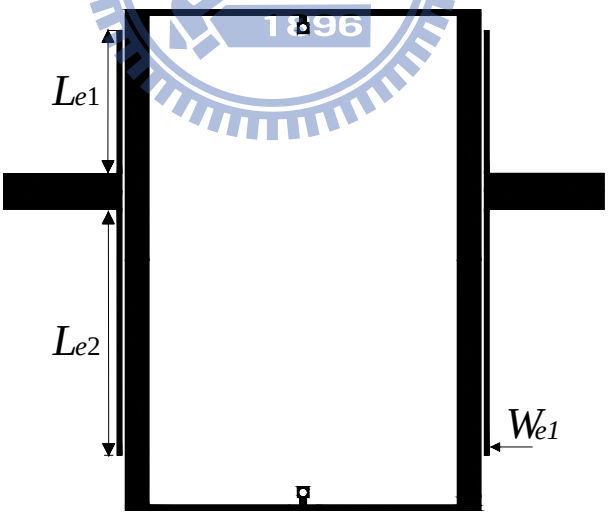

(a)

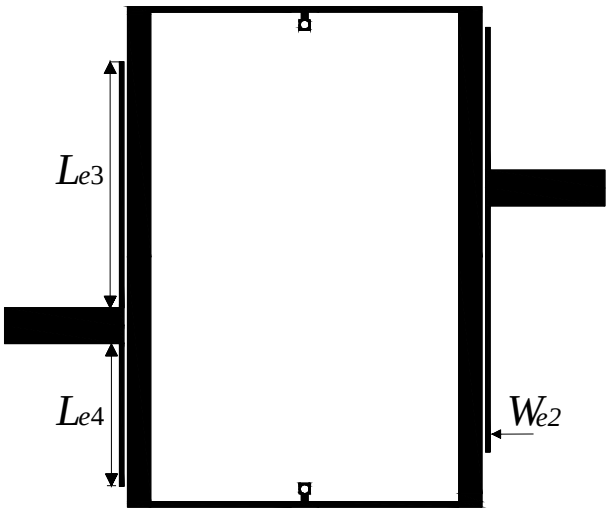

(b)

Fig. 3-7 (a) Circuit layout of symmetric feed-in structure. Geometric parameters in mm: L_{e1} = 6.23, L_{e2} = 10.73. (b) Circuit layout of skew feed-in structure. Geometric parameters in mm: L_{e3} = 10.73 and L_{e4} = 6.23.

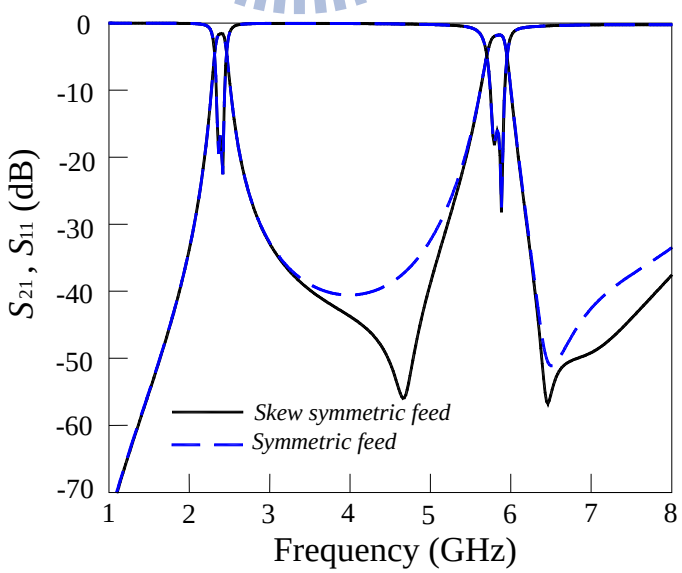

Fig. 3-8 Frequency responses of skew symmetric and symmetric feed structures.

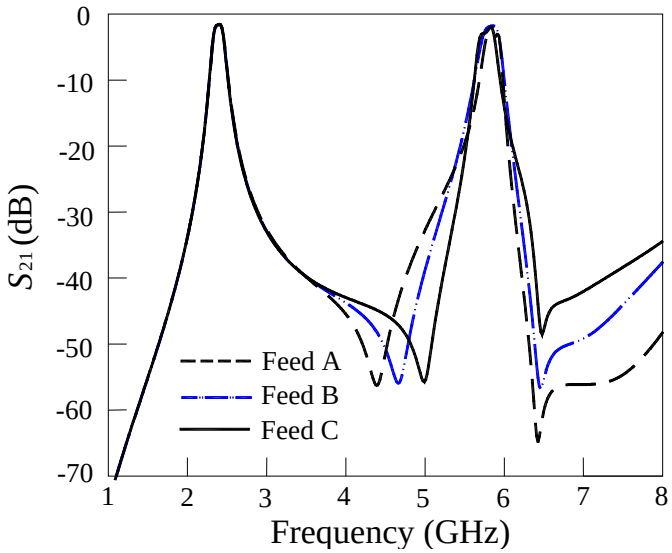

Fig. 3-9 Variations of transmission zeros with respect to different feed locations

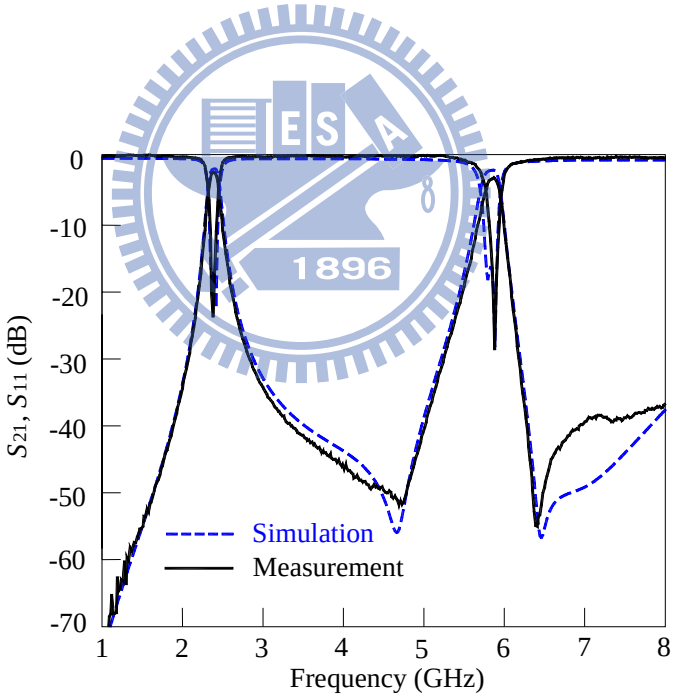

(a)

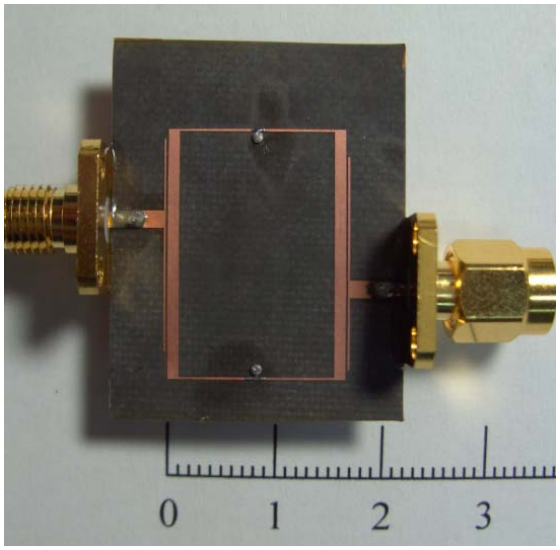

(b)

Fig. 3-10 (a) Simulation and measured results. (b) Circuit photo. Geometric parameters in mm: L_1 = 21.34, W_1 = 1.02, L_2 = 13.4, W_2 = 0.23, W_{t1} = W_{t2} = 0.3, L_{t1} = L_{t2} = 0.35, W_s = 1.55, L_{e1} = 10.725, L_{e2} = 6.225, W_e = 0.15, radius = r = 0.2.

Chapter 4

Dual-mode dual-band bandpass filter (III)

Fig. 4-1 shows a dual-mode dual-band bandpass filter evolved from the circuit in Fig. 3-1 with the quasi-elliptic function response with source-load coupling. To ease the fabricated process, the two separate grounds via in Fig. 3-1 are connected to a single ground via. In this way, the fabricated process becomes simpler than the previous demonstration. Two resonators are folded so that size reduction can be achieved. The two short high-impedance sections and the ground via are equivalent to a T-network with three inductors as shown in Fig. 4-2, since inductive coupling exist among the resonant modes.

4.1 Resonant frequency

The two center frequencies of this design are also at f_1 = 2.45 GHz and f_2 = 5.8 GHz. By selecting proper impedance ratio R and electrical length ratio u in Fig. 3-3, the ratio f_2/f_1 = 5.8/2.45 = 2.367 can be obtained. Since this structure is symmetric, again, even-mode and odd-mode analyses can be applied to calculate the resonant frequencies. The even-mode and odd-mode equivalent circuits of Fig. 4-1 are as shown in Fig. 4-2(a) and Fig. 4-2(b). In Fig. 4-2(a), the even mode input admittance can be written as

$$Y_{ine} = Y_{ine1} + Y_{ine2} \tag{4.1}$$

When Y_{ine} is equal to zero, the even mode condition can be derived as

$$2\omega(L_1 + L_2)(Z_2 + Z_1 \cot\theta_1 \tan\theta_2) - Z_1 Z_2 \cot\theta_1 + Z_2^2 \tan\theta_2 = 0 \tag{4.2}$$

In Fig. 3-4(b), for the odd mode, the input admittance can be written as

$$Y_{ino} = Y_{ino1} + Y_{ino2} \tag{4.3}$$

When Y_{ino} is equal to zero, the odd mode condition can be derived as

$$\omega L_1(Z_2 - Z_1 \tan\theta_1 \tan\theta_2) + Z_1 Z_2 \tan\theta_1 + Z_2^2 \tan\theta_2 = 0 \tag{4.4}$$

4.2 Extraction of the equivalent inductor values

Two short high-impedance sections and ground via can be equivalent to a T-network with three inductors as shown as Fig. 4-1(b). The inductor values of L_1 and L_2 can be extracted in a way similar to that presented in Section 2.2. For a substrate with ε_r = 2.2 and thickness = 0.508 mm, L_1 is about 0.21 nH and L_2 is about 0.06 nH, when L_{t1} = L_{t2} = 0.25 mm, W_{t1} = W_{t2} = 0.3 mm, and r (radius of the ground via) = 0.2 mm. Fig. 4-3 shows the inductor values of L_1

and L_2 with respect to the operating frequencies from 1 GHz to 8 GHz. It can be observed that variations of the inductor values with respect to operating frequencies are quite small. It's noted that the resonant frequencies can be obtained by solving (4.2) and (4.4), when the values of L_1 and L_2 have been found.

4.3 Control of bandwidths

Fig. 4-4 shows the simulation frequency responses by using weak coupling. It shows a total of four resonant peaks f_1, f_2, f_3, and f_4. In this demonstration, the bandwidth control also is achieved by adjusting the inductive coupling. Here, the resonator has impedance ratio Z_2/Z_1 = 2.0 and length ratio $\theta_2/(\theta_1+\theta_2)$ = 0.395. The corresponding parameters evaluated at f_1 = 2.45 GHz are Z_1 = 65 Ω, Z_2 = 130 Ω, θ_1 = 43°, and θ_2 = 28°. In Fig. 4-5, when the short high-impedance section $L_t = L_{t1} = L_{t2}$ is varied from 0.2 to 1.0 mm, the resonant peaks at $f_1$and f_3 shift to the lower frequencies, whereas the peaks at f_2 and f_4 remain almost unchanged. Based on these results, the bandwidths of the two passbands can be easily controlled.

4.4 Source-load coupling

In [5] and [22], the source-load coupling is used to create additional transmission zeros. Similar idea can be applied to this dual-mode dual-band bandpass filter. Source-load coupling

is implemented by a short anti-parallel coupled-line section as shown as Fig. 4-1. Since it is capable of providing one more signal path from the source to the load, extra transmission zeros can be generated between two passbands. The even and odd mode characteristic impedances of this coupled-line are Z_{oe} = 181.3 Ω and Z_{oo} = 92 Ω, respectively. In Fig. 4-6, the structure with the source-load coupling has five transmission zeros; however, the structure without the source-load coupling, there are no transmission zeros. Fig. 4-7 depicts the variation of these zeros versus the length of the coupled-line section, L_c. It's noted that the rejection level of the stopband is enhanced to -30 dB by the transmission zero f_{z5}.

4.5 Simulation and measurement

A bandpass filter with the quasi-elliptic function response is fabricated and measured. The center frequency of the experimental circuit is designed at f_1 = 2.45 GHz and f_2 = 5.8 GHz. The circuits are realized on a substrate with ε_r = 2.2 and h = 0.508 mm. Fig. 4-8 shows the simulated and measured responses. The measured data indicate that the insertion losses at f_1 and f_2 are 1.63 dB and 2.96 dB, respectively, and the inband return losses are better than 15 dB. The two fractional bandwidths are 8.9% and 3.05%, respectively. The circuit photo is in Fig. 4-9, and the circuit size is 13.84 mm × 14.34 mm ($0.153\lambda_g \times 0.16\lambda_g$). Simulation and measurement show the good agreement.

4.6 Comparison of three dual-mode dual-band bandpass filters

Table 4.1 compares the performances and circuit area of three dual-mode dual-band bandpass filters reported in this paper. The first has the smallest circuit area and has relative good rejection between the two passbands. Although the second bandpass filter has the largest circuit area, the isolation between the two passbands is better than -30 dB. In comparison with the second filter, the third one features a lower measured insertion loss at f_{c1}, many more transmission zeros and a smaller circuit area.

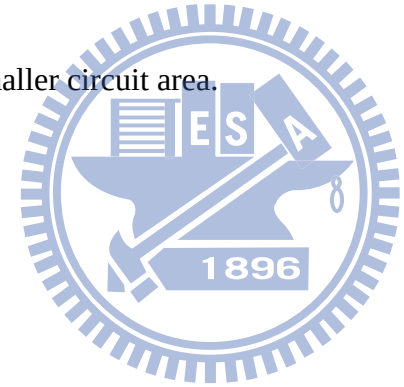

Type	Filter (I)	Filter (II)	Filter (III)
Center frequencies f_{c1} / f_{c2} (GHz)	2.45 / 5.2	2.45 / 5.8	2.45 / 5.8
Insertion loss (measured, in dB)	2.10 / 1.20	2.15 / 2.91	1.63 / 2.96
Max. Insertion loss ($f_{c1} - f_{c2}$)	30 dB	30 dB	15 dB
Number of transmission zeros	4	2	5
Number of via-holes	1	2	1
Circuit area (in mm^2)	11.50 × 16.90	15.44 × 21.80	13.84 × 14.34

Table 4.1 Related parameters of three dual-mode dual-band bandpass filters

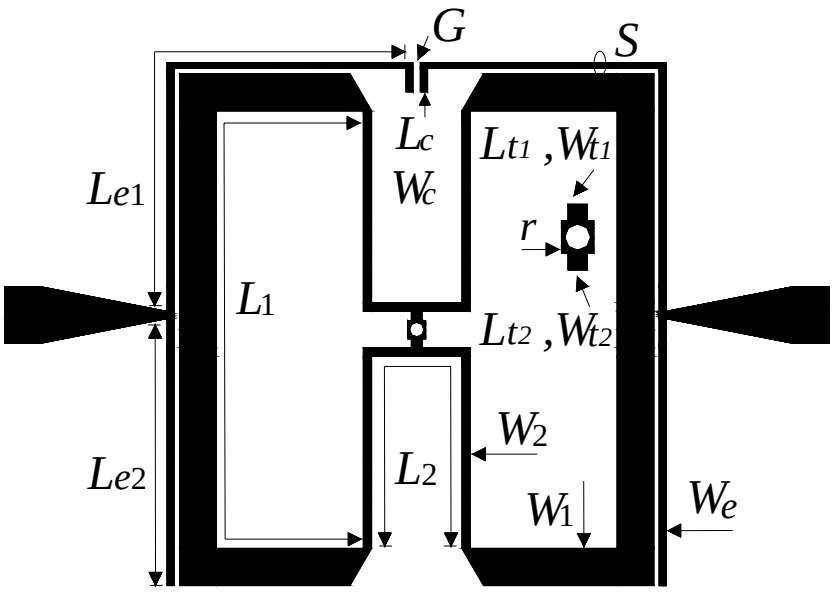

(a)

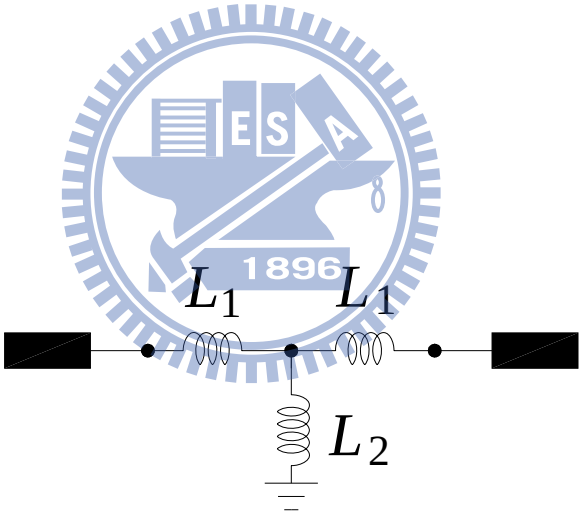

(b)

Fig. 4-1 (a) Circuit layout of the proposed dual-mode dual-band filter. (b) Equivalent circuit of the ground via connected with two short high-impedance sections.

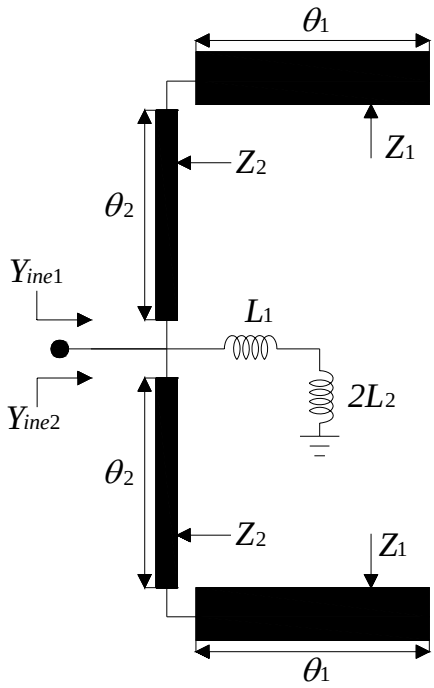

(a)

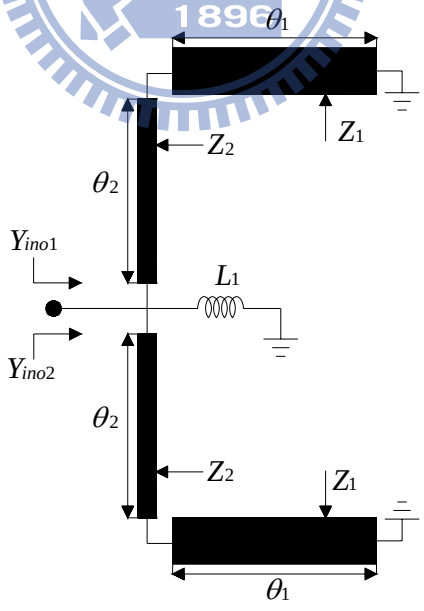

(b)

Fig. 4-2 (a) Even-mode equivalent circuit of Fig. 4-1(a). (b) Odd-mode equivalent circuit of Fig. 4-1(a)

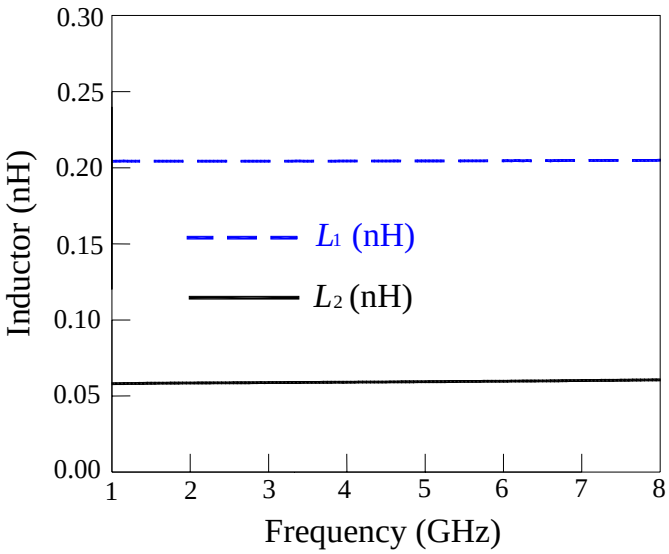

Fig. 4-3 Values of L_1 and L_2.

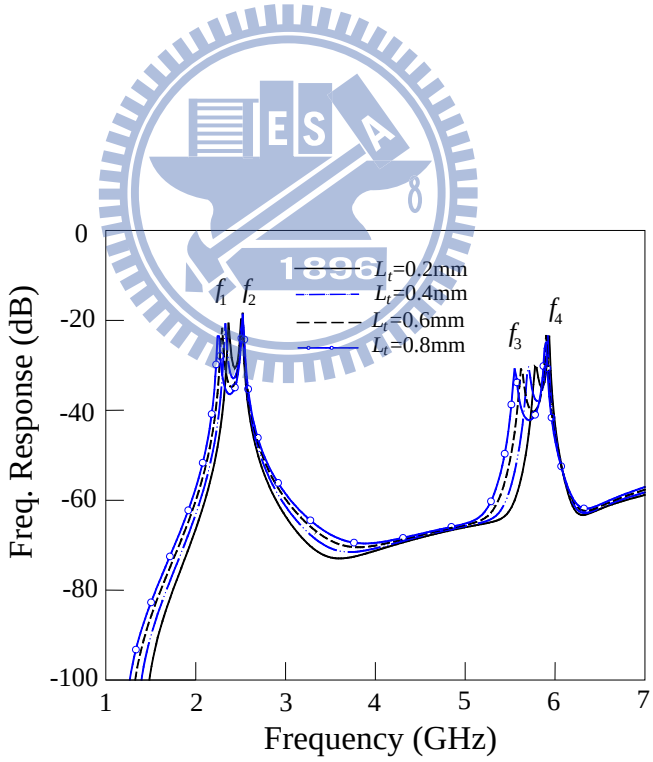

Fig. 4-4 Changes of resonant frequencies with variation of L_t. Detailed parameters are in Fig. 4-9.

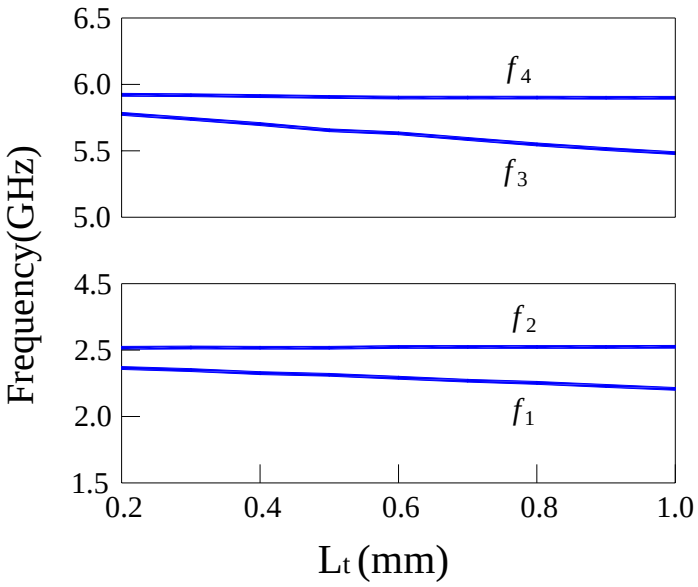

Fig. 4-5 Resonant frequencies versus $L_{t1} = L_{t2} = L_t$. Geometric parameters in mm: $W_t = 0.3$, $r = 0.2$.

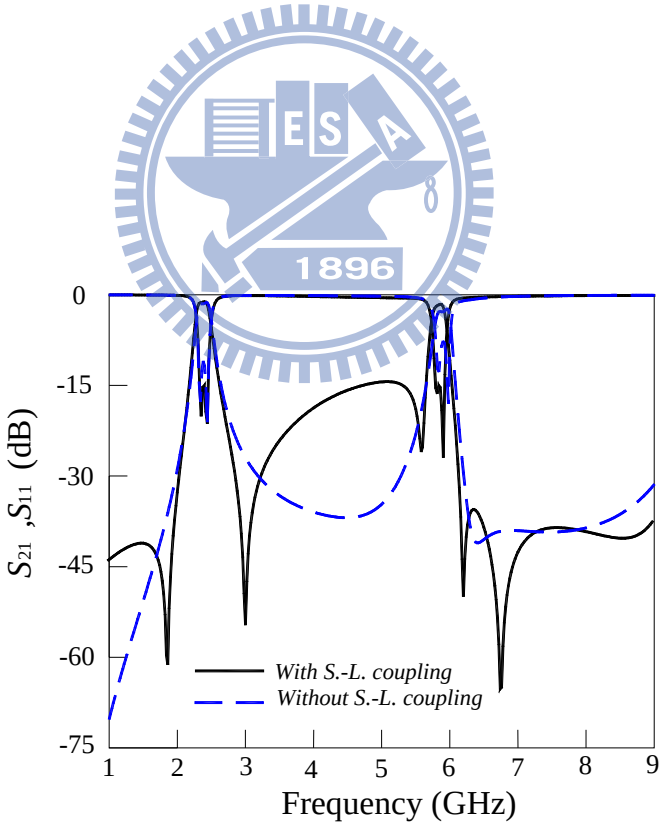

Fig. 4-6 Frequency response of the filter with source-load coupling.

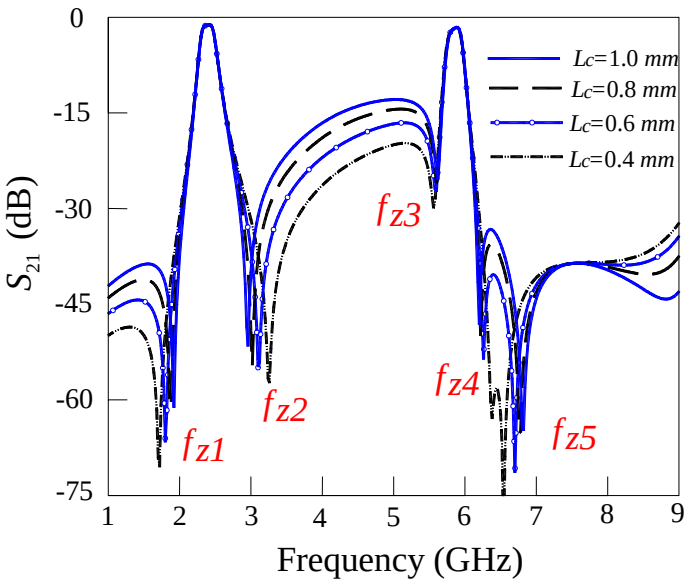

Fig. 4-7 Change of the four transmission zeros versus the length of source-load coupled section, L_c.

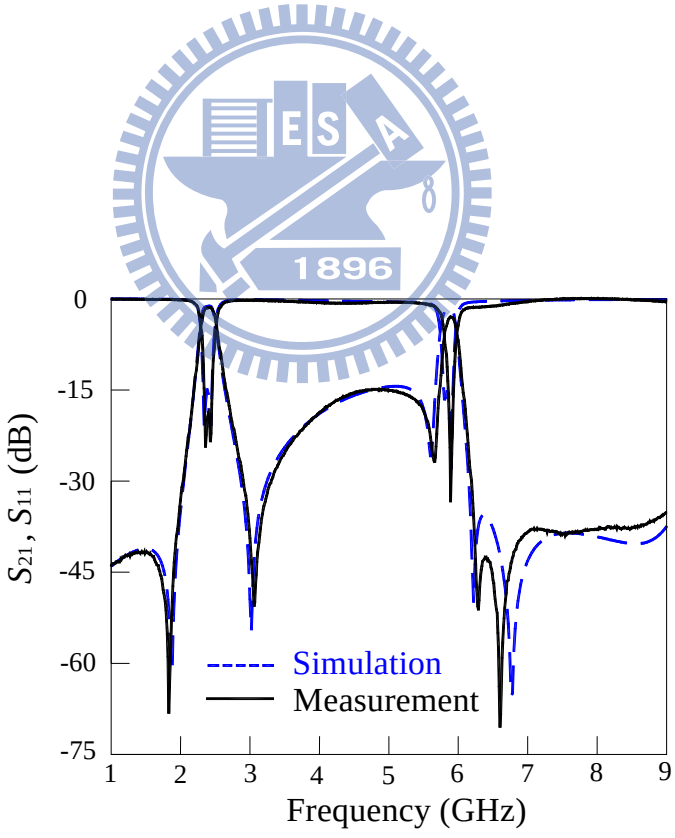

Fig. 4-8 Simulation and measured results.

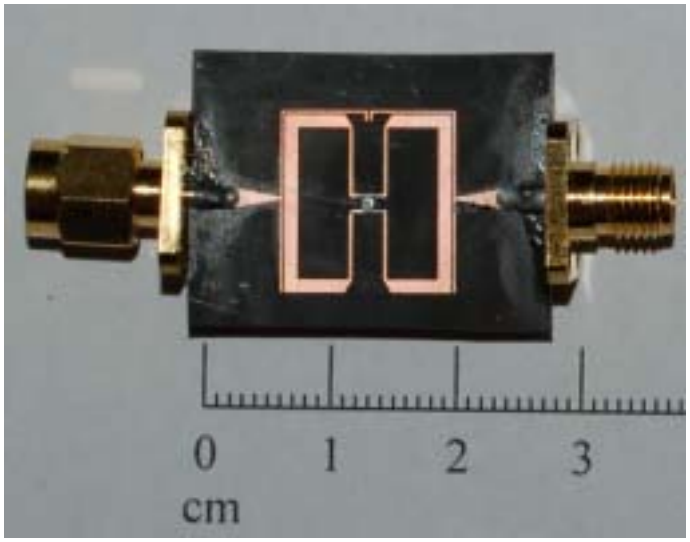

Fig. 4-9 Circuit photo. Geometric parameters in mm: L_1 = 20.14, W_1 = 1.02, L_2 = 13.1, W_2 = 0.23, W_{t1} = W_{t2} = 0.3, L_{t1} = L_{t2} = 0.25, W_c = 0.2, L_c = 0.8, L_{e1} = 13.24, L_{e2} = 7.32, W_e = S = 0.15, G = 0.2, radius = r = 0.2.

Chapter 5
Conclusion

Three dual-mode dual-band bandpass filters with controllable bandwidths are studied in this thesis. The stepped-impedance resonators are used as resonating elements to achieve the dual-band characteristics. By adjusting the inductive and capacitive couplings provided by high-impedance sections and interdigital capacitors, the bandwidth of the two passbands can be well controlled. In addition, additional transmission zeros can be created by employing the source-load coupling and skew symmetric feed structure.

The first dual-mode dual-band bandpass filters composed of a single resonating element are demonstrated. The resonating element is a stepped-impedance resonator with its center being connected to a ground via with a high-impedance section for inductive coupling of the resonant modes. Capacitive coupling is also introduced in shunt with the inductive network for control of the circuit bandwidths at the two designated frequencies. Two extra tunable transmission zeros are created with the source-load coupling by a coupled-line section, leading both passbands to feature quasi-elliptic function responses. Two experimental circuits with different bandwidths are fabricated and measured to demonstrate the design flexibility of the proposed circuit. The simulation and measurement results show good agreement.

The second dual-mode dual-band bandpass filter is demonstrated by alternative

stepped-impedance resonators. To achieve dual-mode operation, the two stepped-impedance resonators are connected to the ground via by two short high- impedance sections. The high-impedance sections and ground via are equivalent to inductors for providing coupling between the resonant modes; therefore, the bandwidths of the two passbands can be controlled by adjusting the inductive coupling. In addition, the skew symmetric feed structure is used to generate two transmission zeros. The simulation and measured data show good agreement.

The third dual-mode dual-band bandpass filter is evolved from the second dual-mode dual-band bandpass filter. In this third dual-mode dual-band bandpass filter, the two ground vias in the previous filter are connected to a single one to ease the fabricated process. A more compact circuit area is obtained at the same time. With the aid of source-load coupling, additional transmission zeros are generated to improved the selectivity of the two passbands. The simulation and measurement results show good agreement.

References

[1] J.-T. Kuo, T.-H. Yeh and C.-C. Yeh, “Design of microstrip bandpass filters with a dual-passband response,” *IEEE Trans. Microwave Theory Tech.*, vol. 53, no. 11, pp. 1331-1337, Apr. 2005.

[2] J.-T. Kuo and H.-P. Lin, “Dual-band bandpass filter with improved performance in extended upper rejection band,” *IEEE Trans. Microwave Theory Tech.*, vol. 57, no. 4, pp. 824-829, Apr. 2009.

[3] J.-T. Kuo and H.-S. Cheng, “Design of quasi-elliptic function filters with a dual-passband response,” *IEEE Microwave Wireless Compon. Lett.*, vol. 14, no. 10, pp. 472-474, Oct. 2004.

[4] C.-H. Tseng and H.-Y. Shao, “A new dual-band microstrip bandpass filter using net-type resonators,” *IEEE Microwave Wireless Compon. Lett.*, vol. 20, no. 4, pp. 196-198, April. 2010.

[5] G.-L. Dai, Y.-X. Guo and M.-Y. Xia, “Dual-band bandpass filter using parallel short-end feed scheme,” *IEEE Microw. Wireles Compon. Lett.*, vol. 20, no. 6, pp. 325–327, Jun. 2010.

[6] M.-H. Wang, H.-W. Wu and Y.-K. Su, “Compact and low loss dualband bandpass filter using pseudo-interdigital stepped impedance resonators for WLANS,” *IEEE Microw. Wireless Compon. Lett.*, vol. 17, no. 3, pp. 187–189, Mar. 2007.

[7] X.-Y. Zhang, J.-X. Cheng, Q. Xue and S. M. Li, “Dual-band bandpass filters using stub-loaded resonators,” *IEEE Microw. Wireles Compon.Lett.*, vol. 17, no. 8, pp. 583–585, Aug. 2007.

[8] P. Mondal and M. K. Mondal, “Design of dual-band bandpass filters using stub-loaded open-loop resonators,” *IEEE Trans. Microw. Theory Tech.*, vol. 56, no. 1, pp. 150–154, Jan. 2008.

[9] C.-M. Tsai, H.-M. Lee and C.-C. Tsai, “Planar filter design with fully controllable second passband,” *IEEE Trans. Microwave Theory Tech.*, vol. 53, no. 11, pp. 3429-3439, Nov. 2005.

[10] H.-M. Lee and C.-M. Tsai, “Dual-band filter design with flexible passband and bandwidth selections,” *IEEE Trans. Microwave Theory Tech.*, vol. 55, no. 5, pp. 1002-1009, May. 2007.

[11] J.-X. Chen, T.-Y. Yum, J.-L. Li and Q. Xue, “Dual-mode dual-band bandpass filter using stacked-loop structure,” *IEEE Microw. Wireless Compon. Lett.*, vol. 16, no. 9, pp. 502-504, Sep. 2006.

[12] X. Y. Zhang and Q. Xue, “Novel dual-mode dual-band filters using coplanar-waveguide-fed ring resonators,” *IEEE Trans. Microw. Theory Tech.*, vol. 55, no. 10, pp. 2183-2190, Oct. 2007.

[13] A. Görür and C. Karpuz, “Compact dual-band bandpass filters using dual-mode resonators,” in *IEEE MTT-S Int. Dig*., Jun. 2007, pp. 905-908.

[14] C. Lugo and J. Papapolymerou, “Multilayer dual-band filter using a reflector cavity and dual-mode resonators,” *IEEE Microw. Wireless Compon. Lett.*, vol. 17, no. 9, pp. 637-639, Sep. 2007.

[15] J.-S. Hong and W. Tang, “Dual-band filter based on non-degenerated dual-mode slow-wave open-loop resonators,” *IEEE MTT-S Int. Microwave Symp. Dig.*, pp. 861–864, Boston, MA, Jun. 2009.

[16] Y.-C. Chiou, C.-Y. Wu and J.-T. Kuo, “New miniaturized dual-mode dual-band ring resonator bandpass filter with microwave *C*-sections,” *IEEE Microwave Wireless Compon. Lett.*, vol. 20, no. 2, pp. 67-69, Feb. 2010.

[17] T.-W. Lin, U.-H. Lok and J.-T. Kuo, “New dual-mode dual-band bandpass filters with quasi-elliptic function passbands and controllable bandwidths,” in *IEEE MTT-S Int. Dig*., Jun. 2010, pp. 905-908.

[18] Q.-X. Chu, F.-C. Chen, Z.-H. Tu and H. Wang, “A novel crossed resonator and its applications to bandpass filters,” *IEEE Trans. Microw. Theory Tech.*, vol. 57, no. 7, pp. 1753-1759, Jul. 2009.

[19] P.-H. Deng, Y.-S. Lin, C.-H. Wang and C.-H. Chen, “Compact microstrip bandpass filters with good selectivity and stopband rejection,” *IEEE Trans. Microw. Theory Tech.*, vol. 54, no. 2, pp. 533-539, Feb. 2006.

[20] L. Athukorala and D. Budimir, “Compact dual-mode open loop microstrip resonators and filters,” *IEEE Microw. Wireless Compon. Lett.*, vol. 19, no. 11, pp. 360-362, Nov. 2009.

[21] C.-M. Tsai, S.-Y. Lee and C.-C. Tsai, “Performance of a planar filter using 0^{o} feed structure,” *IEEE Trans. Microw. Theory Tech.*, vol. 50, no. 10, pp. 2362-2367, Oct. 2002.

[22] W.-H. Tu, “Compact dual-mode cross-coupled microstrip bandpass filter with tunable transmission zeros,” *Microwaves, Antennas & Propagation, IET* , vol. 2, no. 4, pp. 373–377, Jun. 2008.

[23] *IE3D Simulator*, Zeland Software Inc., Jan. 1997.

[24] I. Bahl, *Lumped Elements for RF and Microwave Circuits*. Boston, MA: Artech House, 2003, pp. 230 – 235.

[25] D. M. Pozar, *Microwave Engineering*, 2nd ed. New York: Wiley, 1998.